Light propagation through a sharp-bend coupled-cavity waveguide in a two-dimensional photonic crystal

N. Malkova* and C. Z. Ning†
Center for Nanotechnology, NASA Ames Research Center, Moffett Field, California 94035, USA
(Received 28 September 2005; revised manuscript received 23 February 2006; published 3 April 2006)

We investigate light propagation through a coupled-defect waveguide with a 45° sharp bend in a two-dimensional photonic crystal analytically and numerically. The waveguide mode is the degenerate defect state of a square lattice. The transmission through such a structure drops by two orders of magnitude if a 45° bend is introduced. We show that, by properly distorting the lattice around each defect, the splitting of the degenerate defect state allows resonant transmission through the bend, leading to a two orders of magnitude increase in transmission through the bend waveguide. Several applications of such waveguides are discussed including dynamical directional switching and dynamic light trapping and releasing.

DOI: 10.1103/PhysRevB.73.155101 PACS number(s): 42.70.Qs, 41.20.Jb, 42.79.Gn, 71.70.Ej

I. INTRODUCTION

Photonic crystals have attracted a great deal of interest.[1] By placing a defect within an ideal photonic crystal, a localized resonance peak may be created within the band gap. Photons with a certain wavelength can be locally trapped inside the defect volume. Furthermore, a chain of defects placed within coupling distance forms a mechanism for waveguiding. Two main designs are commonly employed to guide electromagnetic waves in photonic crystal based waveguides. The first design is line defect waveguides, where light is guided along a continuous line of defects.[2] The second design is so-called coupled-cavity waveguides.[3] In such a waveguide, light propagation based on coupling between the localized eigenstates of nearest defects follows the geometrical layout of the defects, allowing the light path to be manipulated on a nanoscale. Therefore, coupled cavity waveguides are considered as a promising candidate for future high-density photonic integrated circuits.

One of the important features of the coupled-cavity waveguides is the possibility of constructing lossless and reflectionless bends.[4,5] It has been assumed[4] that bends can be introduced into the waveguide path by taking advantage of the crystal symmetry without consequential bend reflection loss. It was also reported about the almost perfect transmission through a zigzag chain.[5] However, since a zigzag layout of the defects does not imply the same light path through the crystal, the high transmission through the zigzag chain does not mean a reflectionless transmission through waveguides of arbitrary bending angle. A detailed theoretical analysis based on the tight-binding model showed that reflectionless transmission through the sharp bend can be achieved under a strict set of criteria only.[6] It was shown that the reflection from the bend is governed by the ratio c_1/c_o of the matrix element of the next-nearest-neighbor coupling c_1 to that of the nearest-neighbor coupling c_o. For example, the propagation through 60° bend in the hexagonal lattice results in a significant level of reflection, since in this case $c_1/c_o=1$. Therefore, the reflectionless bend requires a more elaborate design. On the other hand, for application in optical devices, it is important to realize the tunability of the photonic crystals. It is still a challenge to design a photonic crystal based waveguide that allows for controlling the light propagation through any corner.

The aim of this paper is to analyze the light propagation through a 45° bend waveguide. We are particularly interested in a coupled-cavity waveguide based on a square lattice in two dimensions, operating on a degenerate defect state as a guided mode. In recent papers[7,8] we suggested designing complex shaped coupled-cavity waveguides using tunable splitting of the degenerate defect state. The effect used is analogous to the Jahn-Teller effect in solids.[9] It is based on the symmetry analysis of the splitting of degenerate state by a proper distortion of the lattice. The design of the tunable 90° bend[7] and T-shaped[8] coupled-cavity waveguides was proposed. In this paper, we present a design of a tunable 45° bend coupled-cavity waveguide based on a theoretical analysis. We demonstrate that the tunable splitting of the degenerate defect state allows us to control the resonant tunneling through the split states and to tailor the bend with the prescribed value of ratio c_1/c_o. Thereby, we can tune the system to the resonance with almost 100% transmission. We show that the effect used is an effective means for controlling light propagation direction and its velocity in photonic crystal based waveguides.

The paper is organized as follows. In Sec. II, we describe the model system and present numerical and theoretical analysis for the light propagation through the structure. In Sec. III, we describe the design of the waveguide and present the analysis of the structure. Section IV concludes the paper with a summary of the main results.

II. MODEL SYSTEM

As a model structure we consider a square photonic crystal of the dielectric rods, embedded in the air, with the lattice constant a, the radius of the rods $r=0.2a$, and the dielectric constant $\epsilon_r=11.9$. This structure prohibits propagation of TM mode (magnetic field is in-plane and electric field is parallel to the rods) in the frequency range $\tilde{\omega}a/2\pi c=[0.28,0.42]$.[10] Increasing the radius of a single rod to $0.3a$ creates a resonant cavity. This cavity supports a doubly degenerate E state

at the frequency $\tilde{\omega}_o = \omega_o a/2\pi c = 0.358$, which is almost exactly in the middle of the band gap.[10] The degenerate E state of the square lattice is well known[9] to be described by a linear combination of the two states that are similar to the $|p_x\rangle$ and $|p_y\rangle$ states in solids.

Introducing N defects into the crystal and placing them periodically within coupling distance splits each of the degenerate states into N states. Neglecting losses and taking into account the coupling between the nearest neighbors only, we can describe the dynamics of the field amplitude $a_n(t)$ on the n defect in the chain by a set of N ordinary differential equations,[6]

$$i\frac{d}{dt}a_n = \omega_o a_n - c_o(a_{n-1} + a_{n+1}). \tag{1}$$

In the case of the doubly degenerate defect state, this is a matrix equation, with a_n being the 2×1 vector with the components $a_n^{x,y}$ describing the field amplitude of the $|p_{x,y}\rangle$ states. The coupling between the nearest defects is represented by the matrix

$$c_o = \begin{pmatrix} c_{xx} & c_{xy} \\ c_{yx} & c_{yy} \end{pmatrix} \tag{2}$$

with the matrix elements

$$c_{ij} = \omega_o \frac{\int d\vec{r}\,\delta\epsilon \vec{E}_n^i \vec{E}_{n-1}^j}{\int d\vec{r}\epsilon |\vec{E}_n^i|^2}. \tag{3}$$

Here $\vec{E}_n^i$ is the defect mode corresponding to the $|p_i\rangle$ $(i=x,y)$ state, which is localized at the nth site, ϵ is the spatial distribution of the dielectric constant in the single-defect photonic crystal, and $\delta\epsilon$ is the dielectric constant change induced by other defects. In the case of the chain directed along the x or y axis, the coupling integral c_{xy} between the $|p_x\rangle$ and $|p_y\rangle$ states is equal to zero. Hence the matrix equation (1) reduces to two independent sets of N equations. The solution of this problem results in two sets of N levels related to the $|p_x\rangle$ or $|p_y\rangle$ states. Roughly, these levels are separated by c_{xx}/N or c_{yy}/N. Thereby, for a big number N of the defects in the chain such that the separation between the resonant levels is larger than the half-width of the resonant peak determined by the defect quality factor Q, $c_{xx(yy)}/N < Q^{-1}$, the set of the discrete resonant levels generates a quasicontinuous miniband. In direct analogy with the convenient waveguides, the dispersion relation for this miniband will describe the dispersion for a guided mode.[11]

We first analyze the coupled-cavity 45° bend waveguide that is based on our model two-dimensional photonic crystal. The system is shown in Fig. 1. The first waveguide branch (before bending) is along the x axis, and the second branch (after bending) is tilted at 45° from the y axis. The z axis is perpendicular to the figure plane.

In order to analyze this structure, we use the finite-difference time domain (FDTD) technique.[12] Our computational domain is shown in Fig. 1. It contained 14×14 unit cells. Each unit cell was divided into 20×20 discretization

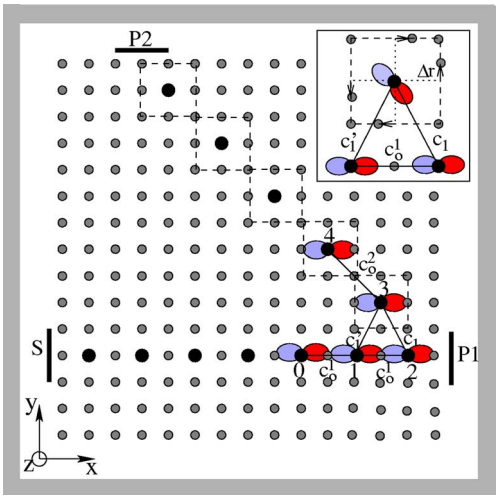

FIG. 1. (Color online) Coupled-cavity 45° bend waveguide studied. The reference system, source (S), two ports ($P1$,$P2$), perfect matched layers, and the corner cell are shown. The inset demonstrates the lattice distortion by the B_2 mode. The coupling matrix elements involved are illustrated, where in red (dark grey) and in blue (light grey) color the positive and negative loops of the p mode are shown, respectively.

grid cells. The computational domain was surrounded by perfect matched layers, with the thickness corresponding to 10 layers of the discretization grid. Each time step was equal to $\Delta t = 1/(2\Delta xc)$. The numerical simulations were performed with the total number of the time steps equal to 100000, 200000, and 300000 in order to check if the stationary regime is reached. A symmetrical Gaussian beam with respect to the x axis was launched at the input of the structure (S in Fig. 1). The width of the beam was equal to 20 grid cells. A frequency spectrum of the source covered the region of interest $\Delta\tilde{\omega} = 0-0.4$. To find the transmission of the structure, we collected the signal at the two output ports ($P1$ and $P2$ in Fig. 1) and compared these data with the reference signal collected at the input of the structure.

The computed transmissions coefficients of the structure at ports 1 and 2 are shown in Figs. 2(a) and 2(b), respectively. The distribution of the z component of the electric field at the resonant frequency $\tilde{\omega} = 0.36$ corresponding to the maximum of the transmission at port 2 is demonstrated in Fig. 2(c). First of all, we note that coupling of the excited wave into the second waveguide branch is very weak. The transmission coefficient at port 2 is two orders of magnitude smaller than at port 1. Second, this coupled-cavity system is described by the discrete levels. They can be considered as eigenvalues of the problem for each of the waveguide branches following from Eqs. (1) with the relevant coupling matrix (2). In agreement with the number of defects involved on each of the branches, the response functions at both ports consist of the same number of peaks. Under the conditions of our numerical experiment, when the source is a symmetrical Gaussian beam (with respect to the x axis), only $|p_x\rangle$ states can be effectively excited. Therefore, the $|p_y\rangle$ states do not contribute to the transmission at port 1. The width of the transmission band at port 1 is mostly determined by the coupling matrix element between the nearest localized $|p_x\rangle$

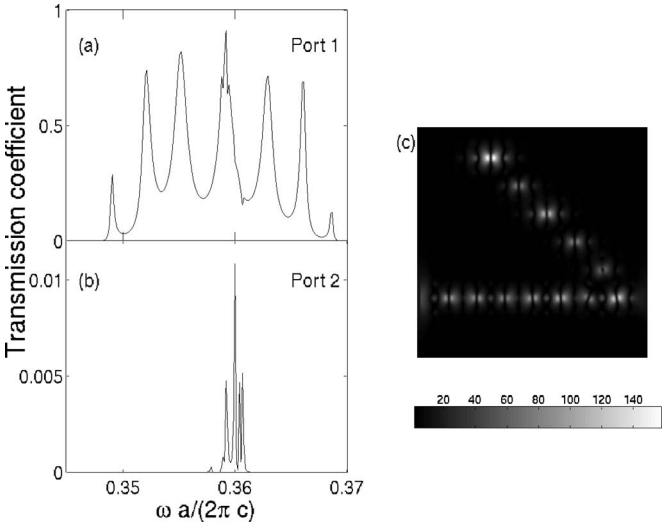

FIG. 2. Computed transmission coefficient of the structure with $\Delta r/a=0$ at ports 1 (a) and 2 (b); (c) the distribution of $|E_z|$ field at the resonant frequency corresponding to the maximum of the transmission at port 2.

states, denoted as $c_o^1=c_{xx}$ in Fig. 1. It is interesting to note that in the middle of the transmission band, the peaks are wider and higher than in the edge region. The reason for this is that the excited wave in the middle of the band has the biggest group velocity and therefore it will decay most quickly,[6] while at the band edge, the group velocity of the wave goes to zero resulting in infinitely long decay time and narrow resonant peak. Unavoidable losses (the reflection from the crystal boundaries) reduce the overall transmission and wash out the fine structure of the response function.

The transmission band of the second branch, or the response function at port 2, can also be described by the set of Eqs. (1) with the coupling matrix c_o^2 shown in Fig. 1. However, in this case, the matrix elements $c_{xy}\neq 0$. Therefore in general, set (1) contains $2N$ equations. However, in the particular case of our numerical experiment, the symmetrical Gaussian beam can excite only the $|p_x\rangle$ states on the first branch. Then, we assume that only $|p_x\rangle$ states are launched into the second branch. Accordingly, we neglect the coupling between the $|p_x\rangle$ and $|p_y\rangle$ states at the second branch also. This assumption is supported by the field distribution in Fig. 2(c).

Comparing Figs. 2(a) and 2(b), we can see that the transmission band at port 2 is much narrower than the band of the first branch. The reason for this is that the coupling coefficient between the nearest $|p_x\rangle$ defect states on the second branch, c_o^2, is much smaller than the coupling between the $|p_x\rangle$ states at the first branch, c_o^1. We can roughly estimate the ratio c_o^2/c_o^1 using the tight-binding model developed for solids[13].

Any $|p\rangle$ orbital can be decomposed into the component oriented along the coupling direction, the so-called σ component, and the mutually perpendicular component, the π component. Accordingly, the coupling matrix elements between the $|p\rangle$ states can be decomposed into the σ- and π-coupling matrix elements, denoted as V_σ and V_π, respectively. In the case of the atomic orbitals, both matrix elements scale with the distance d between the two localized orbitals, $V_{\sigma,\pi}\sim \eta_{\sigma,\pi}/d^2$, where $\eta_{\sigma,\pi}$ are constants, which are in general considered as empirical parameters. The scaling law for solids is obtained by matching the tight-binding cosine dispersion and free-electron parabolic dispersion. Since in both limits of tight-binding and "free-photon" approximations, the dispersion of the coupled-cavity photon system is similar to the dispersion of solids,[3] we assume that, as the first-order approximation, the scaling law can be applied to photonic crystal also. By denoting $V_{\sigma,\pi}^1$ and $V_{\sigma,\pi}^2$ as coupling matrix elements for the first and second branches, respectively, we get

$$c_o^1 = V_\sigma^1,$$

$$c_o^2 = V_\sigma^2\cos^2(\pi/4) + V_\pi^2\sin^2(\pi/4). \tag{4}$$

Taking into account the distance between defects in both waveguide arms, we can estimate $V_{\sigma,\pi}^2/V_{\sigma,\pi}^1\sim 1/2$ and $c_o^2=1/4(V_\sigma^1+V_\pi^1)$. Following the analogy with solids further, we assume that $V_\pi<V_\sigma$ and $V_\pi V_\sigma<0$. We finally obtain

$$c_o^2/c_o^1 < 1/4. \tag{5}$$

Independent estimation of this ratio can be obtained from the FDTD experiment [Figs. 2(a) and 2(b)] as a ratio between the widths of the transmitted bands at both ports. It gives $c_o^2/c_o^1\sim 0.2$. We believe that such a good agreement between the theoretical estimate and the FDTD experiment validates the used assumptions.

From Figs. 2(a) and 2(b), we note that the transmission band of the second waveguide branch overlaps with the central resonant peak of the first branch. It would seem that resonant tunneling between the branches is possible. However, from Fig. 2(b) we see that the coupling of the excited light into the second branch is very weak. In order to explain this, we analyze the coupling matrix elements between the $|p_x\rangle$ states of the corner cell, shown in Fig. 1. The coupling matrix element between defects 2 and 3, denoted as c_1, is exactly equal to the matrix element between defects 1 and 3, denoted as c_1' (Fig. 1). In terms of the tight-binding model,[13] they are expressed as

$$c_1 = c_1' = \tilde{V}_\sigma\cos^2\alpha + \tilde{V}_\pi\sin^2\alpha, \tag{6}$$

where $\tilde{V}_{\sigma,\pi}$ are the σ- and π-matrix elements for the corner cell, and $\cos\alpha=1/\sqrt{5}$. By making use of the scaling law for the coupling matrix elements, we can estimate $\tilde{V}_{\sigma,\pi}/V_{\sigma,\pi}^1\sim 4/5$. Therefore, $c_1=c_1'=4/25c_o^1$. Using relation (5) we get

$$c_1 = c_1' \sim c_o^2. \tag{7}$$

This means that the photon trapped at defect 3 will have an equal probability to move forward to defect 4, or backward to defects 1 and 2 (Fig. 1). This fact should have a direct consequence on the transmitted power at port 2.

This intuitive explanation is supported by a detailed theoretical analysis based on the evolution equations for all the defects of the corner cell,[6]

$$i\frac{d}{dt}a_2 = \omega_o a_2 - c_o^1 a_1 - c_1 a_3,$$

$$i\frac{d}{dt}a_1 = \omega_o a_1 - c_o^1(a_o + a_2) - c_1' a_3,$$

$$i\frac{d}{dt}a_3 = \omega_o a_3 - c_o^2 a_4 - c_1 a_2 - c_1' a_1. \quad (8)$$

For a monochromatic excitation, the field before the bend ($n<2$) consists of incident and reflected components

$$a_n = a_{in}\exp[i\alpha_1(n-1) - i\omega t] + a_\rho \exp[-i\alpha_1(n-1) - i\omega t],$$

and only the transmitted fields leave the corner defect ($n>2$),

$$a_n = a_\tau \exp[i\alpha_2(n-2) - i\omega t].$$

The wave numbers $\alpha_{1,2}$ are related to the dispersion relations on the two waveguide branches as follows:

$$\omega = \omega_o - 2c_o^{1,2}\cos(\alpha_{1,2}).$$

Solution of this problem under condition (7) gives the reflection from the corner at $\omega=\omega_o$,

$$\rho = \left|\frac{a_\rho}{a_{\text{in}}}\right| = \sqrt{\frac{4+[1-(c_o^2/c_o^1)^2]^2}{4+[1+(c_o^2/c_o^1)^2]^2}}. \quad (9)$$

Using the estimation $c_o^2/c_o^1 \sim 0.2$, we get that reflection from the 45° bend reaches 97%. We also note that in the case of the 60° bending $c_o^2/c_o^1=1$, the reflectivity reaches 50%, which agrees with the calculation performed in Ref. 6. Therefore the next-nearest-neighbor interaction along with the mismatch between the transmitted bands of the two branches causes huge losses at port 2. As a result, the 45° bend is almost nontransmissive if no special design is made.

III. DESIGN OF A TUNABLE WAVEGUIDE

At this point we can conclude that, in order to control the light propagation through any corner, we have to find a way of controlling the coupling of the defects in the corner cell. We expect that for $c_1' \ll c_1$, the photon with the certain frequency could effectively propagate to port 2. In a previous paper[8] it was shown that the splitting of the degenerate defect state can be controlled by both magnitude and symmetry of the perturbation potential used. It was proven that the doubly degenerate E state of a square lattice can be split into the states either with the symmetry $|p_x\rangle$ and $|p_y\rangle$ or $|p_\perp\rangle = |p_x + p_y\rangle$ and $|p_\parallel\rangle = |p_x - p_y\rangle$ by means of the perturbation of the B_1 or B_2 modes, respectively. For the geometry of the 45° bend waveguide studied, we have only one choice of surrounding each of the defects in the second waveguide branch by a flexible Jahn-Teller cell distorted by the B_2 mode as shown in the inset of Fig. 1. Thereby, the degenerate state of the defects in the second branch will be split into the $|p_\parallel\rangle$ and $|p_\perp\rangle$ states with the eigenfunctions directed parallel and perpendicular to the second branch, respectively. The frequency splitting $\Delta\omega$ is a linear function of the lattice distortion Δr. By doing this, we can first control the coupling of the defects in the corner cell. Second, we can split the degenerate transmission band of the second branch into two bands with the symmetry of the $|p\rangle$ states parallel and perpendicular to the branch direction. Third, we can control the coupling matrix element and thereby the group velocity for the guided mode of the second branch.

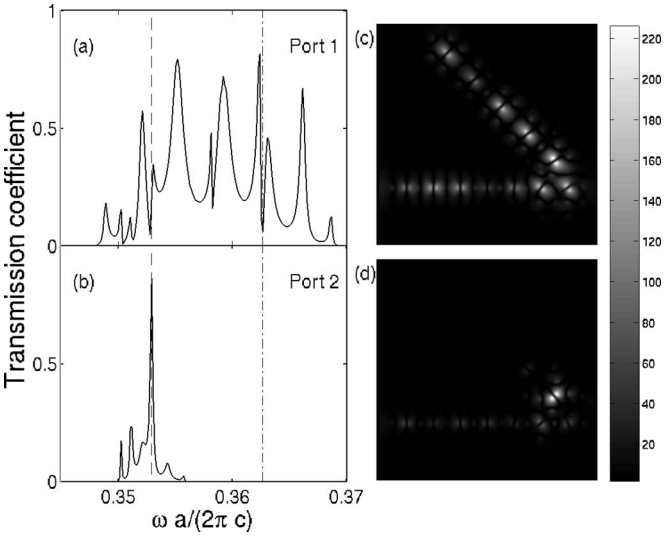

FIG. 3. Computed transmission coefficient of the structure at $\Delta r/a=0.18$ at ports 1 (a) and 2 (b); the distribution of $|E_z|$ field at the resonant frequencies $\tilde{\omega}=0.353$ (c) and 0.363 (d). Frequency $\tilde{\omega}=0.353$ corresponds to the maximum of the transmission at port 2 and "drop-off" frequency at port 1 (dashed line); frequency 0.363 corresponds to the "drop-off" frequency of the transmission at port 1 (dashed-dotted line).

The results of our design are summarized in Figs. 3 and 4. We found that the best transmission of the structure at port 2 is reached at 18% distortion of the second branch. The computed transmission coefficient of the structure with $\Delta r = 0.18a$ at ports 1 and 2 is demonstrated in Figs. 3(a) and

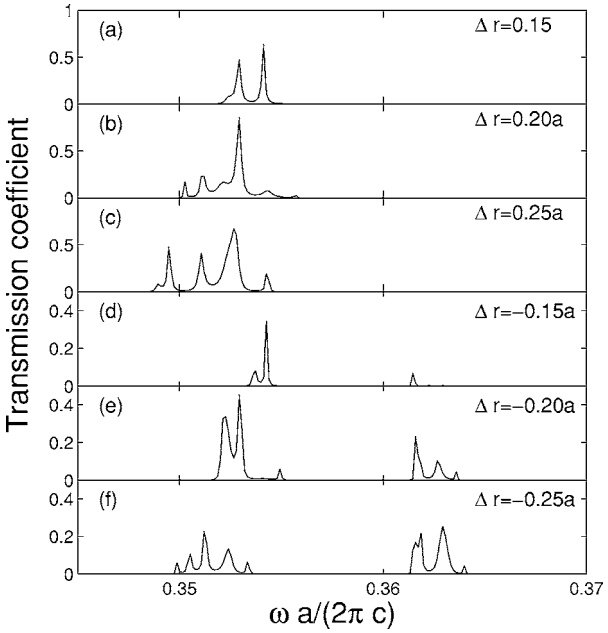

FIG. 4. Transmission coefficient of the structure at port 2 with $|\Delta r|/a=0.15$, 0.2, and 0.25 at $\Delta r>0$ [(a)–(c)] and $\Delta r<0$ [(d)–(f)].

3(b), respectively. In Fig. 3(a), we mark two "drop-off" modes of the transmission at port 1 at $\tilde{\omega}=0.353$ (dashed line) and 0.363 (dashed-dotted line). The distributions of the z component of the electric field at the resonant frequencies $\tilde{\omega}=0.353$ and 0.363 are shown in Figs. 3(c) and 3(d), respectively. Figure 4 presents the transmission coefficient of the structure with $|\Delta r|/a=0.15$, 0.20, and 0.25. The cases of $|\Delta r|/a>0$ and $|\Delta r|<0$ are shown in Figs. 4(a)–4(c) and in Figs. 4(d)–4(f), respectively.

First we note that at $\Delta r=0.18a$, the transmission at port 2 shows a sharp maximum at $\tilde{\omega}\sim 0.353$. Correspondingly, the transmission at port 1 drops down at the same frequency. The transmitted power depends on lattice distortion, reaching the maximum at $\Delta r=0.18a$ [Figs. 3(b) and 4]. Second, the transmission band at port 2 for the distorted lattice is shifted in frequency with respect to the undistorted lattice [compare Fig. 2(b) and 3(b)]. Moreover, the magnitude of the shift is proportional to the magnitude of the distortion (Fig. 4). Some of the peaks of the transmission band at port 1 are split [Fig. 3(a)]. Third, the guided mode of the structure keeps $|p_x\rangle$ symmetry on the first branch before bending and $|p_x-p_y\rangle$ symmetry on the second branch after bending (inset in Fig. 1). The "drop-off" frequency in the transmission band at port 1 corresponds to the $|p_x+p_y\rangle$ state [Fig. 3(d).

We explain these findings in terms of the tight-binding model again. The two waveguide branches are connected through the corner cell shown in Fig. 1. Let us consider first the corner cell itself. The coupling of the doubly degenerate $|p\rangle$ states localized at the three defects results in six eigenstates. The eigenvalues and eigenfunctions of these states can be controlled by the lattice distortion. The role of the corner cell in the transmission properties of the entire structure will be first to provide the resonant tunneling between the two waveguide branches and second to control the symmetry of the nearest neighbors and, thereby, their coupling. Therefore, the resonant transmission at port 1 is reached as soon as the eigenstate of the corner cell with the proper symmetry matches in frequency with the resonant peaks in both waveguide arms. By examining the symmetry of the p states at the resonance frequency shown in Fig. 3(c), we note that in this case, the coupling matrix elements c_1 and c_1' are not equal anymore. Using the tight-binding theory, we find

$$c_1 = 4/5(V_\sigma^1 \cos^2\theta + V_\pi^1 \sin^2\theta),$$

$$c_1' = 4/5(V_\sigma^1 \sin^2\theta + V_\pi^1 \cos^2\theta), \tag{10}$$

where $\tan(\theta+\pi/4)=2$. Taking into account that $V_\sigma \gg V_\pi$, we get $c_1 \sim 9c_1' > c_1'$. This implies that once the photon with the resonant frequency reaches the corner defect 3, it has a much bigger probability to reach port 2 than to come back to defect 1. Therefore, the transmission coefficient at port 2 increases to almost 100% while that at port 1 drops to 0 [dashed line in Figs. 3(a) and 3(b)]. A similar analysis shows that in the case of the second "drop-off" frequency [Fig. 3(d)], $c_1 \sim c_1' \sim c_o^1$. The photon mode with such a frequency is trapped at the corner cell [see Fig. 3(d)], and therefore drops down from the response functions at both ports.

The distortion of the second branch by the B_2 mode results in the splitting of the degenerate E state at each defect into the $|p_\parallel\rangle$ and $|p_\perp\rangle$ states, with the magnitude of the splitting being a linear function of the lattice distortion.[8] We define the lattice distortion as shown in the inset of Fig. 1 to be positive. For $\Delta r>0$, the state $|p_\parallel\rangle$ with the eigenfunction directed along the second waveguide branch decreases in frequency, while the mutually orthogonal state $|p_\perp\rangle$ increases in frequency, and vice versa for $\Delta r<0$. Interaction between $|p_\parallel\rangle$ and $|p_\perp\rangle$ states is prohibited by symmetry. Therefore, the coupling matrix (2) in (1) will be diagonal with the matrix elements $c_\parallel$ and $c_\perp$, describing the coupling between the $|p_\parallel\rangle$ and $|p_\perp\rangle$ states, respectively. In terms of the tight-binding model,[13] the coupling constants can be directly expressed through the π and σ components

$$c_\parallel = V_\sigma^2,$$

$$c_\perp = V_\pi^2. \tag{11}$$

However, since the lattice distortion must strongly affect the empirical parameters $\eta_{\sigma,\pi}$ for the distorted lattice, we can hardly use the scaling law connecting $V_{\sigma,\pi}^2$ with $V_{\sigma,\pi}^1$. Moreover, as will be shown below, the V_σ and V_π matrix elements depend on both the sign and magnitude of the distortion.

Increase in the magnitude of the distortion to $\Delta r>0.08$ first removes the overlap between the transmission bands of the second branch and moves them away from each other. We can follow in Fig. 4 how the transmission bands of the second branch scan the transmission band of the first branch with an increase in the magnitude of the lattice distortion. We also note in Fig. 4 that the response function at port 2 depends on the lattice distortion both in terms of transmitted frequency and intensity. The transmission at port 2 is at maximum at $\Delta r=0.18$. That is a distortion when the eigenstate of the corner cell which satisfies the condition $c_1 \gg c_1'$ overlaps simultaneously with the transmitted band of the second branch and with one of the resonant peaks of the first branch.

In support of this intuitive explanation, we performed an analytical analysis of the corner cell based on Eqs. (8). In the case of distorted structure, the frequency ω_o of defect 3 should be replaced by $\omega_o \pm \Delta\omega$, depending on the sign of the lattice distortion. In numerical analysis of set (8) we assumed that $c_1'=c_1/9$ and $c_1=c_o^2$. Using the results of the FDTD experiment (discussed below), we set $c_o^2=0.6c_o^1$ for the case of distorted structure. This analysis shows that the reflection from the corner is reduced to 10% in the frequency range $\omega=\omega_o-\Delta\omega\pm c_o^2$, when the magnitude of splitting $\Delta\omega\sim c_o^1/2$. As follows from the previous analysis,[8] the frequency splitting $\Delta\omega=c_o^1/2$ caused by the B_2 mode can be achieved with $\Delta r\sim 0.2$. This estimation perfectly agrees with the results of the numerical experiment. It is important to note that reflection from the corner can be decreased even more by increasing the ratio c_o^2/c_o^1. Reflectionless transmission through the bend is reached at $c_o^2/c_o^1=1$, which corresponds to the 60^o bending angle.

However, it was surprising that the response function at port 2 consists of both $|p_\parallel\rangle$ and $|p_\perp\rangle$ bands only for $\Delta r<0$ with the peaks smaller and larger than the frequency $\tilde{\omega}=0.36$, respectively (Fig. 4). But only the $|p_\parallel\rangle$ band is seen for $\Delta r>0$ [Figs. 4(a)–4(c)]. The explanation of this effect

lies in the strong dependence of the spatial confinement of the split states on the lattice distortion. At $\Delta r>0$, the lattice distortion by the B_2 mode redistributes the dielectric rods in such a way that the nearest neighbors become closer to the $|p_\perp\rangle$ state than to the $|p_\parallel\rangle$ state. This results in much stronger localization of the $|p_\perp\rangle$ state than the $|p_\parallel\rangle$ state. The FDTD calculations for the one defect crystal distorted by the B_2 mode with $\Delta r>0$ showed that the $|p_\parallel\rangle$ state spreads much further from the defect than the $|p_\perp\rangle$ state.[10] The $|p_\perp\rangle$ state seems to be screened by the distorted nearest neighbors. The effect increases with the magnitude of the lattice distortion. The wide spread of the $|p_\parallel\rangle$ states results in their strong interaction, thereby giving rise to a wide transmission band. When tuned to resonance with a proper state of the corner cell, the $p_\parallel$ band reveals itself in the maximum transmission at port 2. Since the coupling of the $|p_\perp\rangle$ states at $\Delta r>0$ is very weak, the $p_\perp$ band is not observed in the transmission at port 2 but it reveals itself in the "drop-off" frequency in the transmission at port 1 [Figs. 3(a) and 3(d)].

The situation will be exactly reversed for $\Delta r<0$. In this case, because of the layout of the defects, the coupling between the $p_\parallel$ and $p_\perp$ states will be comparable in magnitude. Therefore, for $\Delta r<0$, both modes contribute to the response function [Figs. 4(d)–4(f)]. However, we note from Fig. 4 that at $\Delta r<0$ the transmitted intensity for both $p_\parallel$ and $p_\perp$ bands is less than that for the $p_\parallel$ band at $\Delta r>0$.

This analysis was supported by the FDTD simulations. We examined the coupling between the defects on the distorted second waveguide branch. It was found that for $\Delta r>0$ the ratio $c_\perp/c_\parallel<1$, which decreases as lattice distortion Δr increases. The magnitude $c_\perp/c_\parallel$ changes from 1/4 at $\Delta r=0.1$ to 1/30 at $\Delta r=0.2$, while for the opposite distortion $\Delta r<0$, $c_\perp/c_\parallel>1$. The value of $c_\perp/c_\parallel$ does not change so drastically: $c_\perp/c_\parallel=3.4$ and 2.4 at $\Delta r=0.1$ and 0.2, respectively. We were also able to estimate the quality factors of the split state using the resonant peaks. It is important to note that the group velocity of the guided mode in a coupled-cavity waveguide is directly proportional to the coupling matrix element.[4] Therefore, control of the coupling matrix element through the lattice distortion could be used to control light velocity in a photonic crystal based waveguide.

IV. CONCLUSION

We studied theoretically and numerically the transmission through a sharp 45° bend based on coupled-cavity waveguide in a two-dimensional photonic crystal. Theoretical analysis showed that the reflection from the corner is determined by the coupling matrix elements of the corner cell. Therefore, in order to control the light propagation through the sharp corner, we have to control the coupling of the defects in the corner cell. We design the photonic crystal based waveguide operating on the degenerate p state, in which the nearest neighbors to the defects in the second branch are distorted by the so-called B_2 lattice distortion. This allows us first to control the coupling of the defects in the corner cell to achieve the control of light propagation through the whole structure. Second, the lattice distortion results in splitting of the degenerate transmission band of the second branch into two bands with the symmetry of the $|p\rangle$ states parallel and perpendicular to the branch direction. We showed that the coupling matrix element depends strongly on the magnitude and sign of the lattice distortion. Since the group velocity of the guided mode in a coupled-cavity waveguide is directly proportional to the coupling matrix element, the ability of controlling the coupling matrix element could be used as an effective means of controlling light velocity in photonic crystals.

Our results for the 45°-bend waveguide can be also used for dynamical control of light propagation. In order to control light propagation dynamically, two possible designs could be suggested. The first is to surround each of the defects of the second waveguide branch by movable rods, so that the resonant transmission can be tuned by a dynamic lattice distortion at each defect. The second design is to build in a static or permanent lattice distortion for all the defects in the second branch except the corner cell and to dynamically tune the lattice distortion of the corner defect only.[14] The frequency of the corner defect can be tuned to resonance, for example by a piezoelectric element built directly beneath or above the waveguide corner.[7] Such switching requires precise control of the positions of rods involved and may present a challenge for the current technology. In our recent paper[15] we have shown that the tuning of the corner defect can also be achieved by using the linear electro-optical effect of the nearest neighbors to the corner defect made of noncentrosymmetrical materials. The dynamical control of the corner cell could open an alternative mechanism for trapping and releasing light of the certain wavelength.[16] In connection with the waveguide studied, frequency $\tilde{\omega}=0.363$ corresponds to the "drop-off" frequency at both ports, for the distorted structure [see Figs. 3(a) and 3(b)]. Hence this mode is trapped at the corner defect when the structure is distorted by an applied electric field [see Fig. 3(d)]. The same mode is released to port 1 as soon as the external electric field is off and the structure restores its symmetry [Fig. 2(a)].

It is important to note that the theoretical analysis presented was based on the assumption that only the $|p_x\rangle$ mode is excited under condition of the numerical experiment. Hence we were able to neglect the coupling between the $|p_x\rangle$ and $|p_y\rangle$ modes. However, in the real experiment this assumption might not be valid, and coupling between the two modes must be taken into account directly. We are going to discuss coupling effects between the two modes in a coupled-cavity bend photonic crystal in our future publication.

*Electronic address: nmalkova@mail.arc.nasa.gov
†Electronic address: cning@mail.arc.nasa.gov

[1] *Photonic Band Gap Materials*, Vol. 315 of NATO Advanced Study Institute, edited by C. M. Soukoulis (Kluwer-Academic, Dordrecht, 1996).
[2] A. Mekis, J. C. Chen, I. Kurland, S. Fan, P. R. Villeneuve, and J. D. Joannopoulos, Phys. Rev. Lett. **77**, 3787 (1996).
[3] N. Stefanou and A. Modinos, Phys. Rev. B **57**, 12127 (1998).
[4] A. Yariv, Y. Xu, R. K. Lee, and A. Scherer, Opt. Lett. **24**, 711 (1999).
[5] M. Bayindir, B. Temelkuran, and E. Ozbay, Phys. Rev. B **61**, R11855 (2000).
[6] U. Peschel, A. L. Reynolds, B. Arredondo, F. Lederer, P. J. Roberts, T. F. Krauss, and P. J. I. de Maagt, IEEE J. Quantum Electron. **38**, 830 (2002).
[7] N. Malkova, S. Kim, and V. Gopalan, Appl. Phys. Lett. **83**, 1509 (2003); N. Malkova and V. Gopalan, J. Phys.: Condens. Matter **16**, 1523 (2004).
[8] N. Malkova and V. Gopalan, Phys. Rev. B **68**, 245115 (2003).
[9] L. D. Landau and E. M. Lifshitz, *Quantum Mechanics* (Nauka, Moscow, 1974).
[10] N. Malkova, S. Kim, and V. Gopalan, Phys. Rev. B **68**, 045105 (2003).
[11] Y. Xu, R. K. Lee, and A. Yariv, J. Opt. Soc. Am. B **17**, 387 (2000).
[12] A. Taflove and S. C. Hagness, *Computational Electrodynamics: The Finite Difference Time Domain Method* (Artech House, Boston, 2000).
[13] W. S. Harrison, *Elementary Electronic Structure* (World Scientific, Singapore, 1999).
[14] N. Malkova and C. Z. Ning, Proc. SPIE **5733**, 159 (2005).
[15] N. Malkova and C. Z. Ning, J. Opt. Soc. Am. B (to be published).
[16] M. F. Yanik, W. Suh, Z. Wang, and S. Fan, Phys. Rev. Lett. **93**, 233903 (2004).